PCP
PLANT & CELL PHYSIOLOGY

Mapping of the Classical Mutation *rosette* Highlights a Role for Calcium in Wound-Induced Rooting

Abelardo Modrego[1], Taras Pasternak[2], Moutasem Omary[1], Alfonso Albacete[3], Antonio Cano[4], José Manuel Pérez-Pérez[2] and Idan Efroni[1,*]

[1]The Institute of Plant Sciences and Genetics in Agriculture, Faculty of Agriculture, The Hebrew University, Rehovot 7610001, Israel
[2]Instituto de Bioingeniería, Universidad Miguel Hernández, Elche 03202, Spain
[3]Departamento de Nutrición Vegetal, CEBAS-CSIC, Murcia 30100, Spain
[4]Departamento de Biología Vegetal (Fisiología Vegetal), Universidad de Murcia, Murcia 30100, Spain

*Corresponding author: E-mail, idan.efroni@mail.huji.ac.il
(Received 10 January 2022; Accepted 17 November 2022)

Regular Paper

Removal of the root system induces the formation of new roots from the remaining shoot. This process is primarily controlled by the phytohormone auxin, which interacts with other signals in a yet unresolved manner. Here, we study the classical tomato mutation *rosette* (*ro*), which lacks shoot-borne roots. *ro* mutants were severely inhibited in formation of wound-induced roots (WiRs) and had reduced auxin transport rates. We mapped *ro* to the tomato ortholog of the *Arabidopsis thaliana BIG* and the mammalians *UBR4/p600*. RO/BIG is a large protein of unknown biochemical function. In *A. thaliana, BIG* was implicated in regulating auxin transport and calcium homeostasis. We show that exogenous calcium inhibits WiR formation in tomato and *A. thaliana ro/big* mutants. Exogenous calcium antagonized the root-promoting effects of the auxin indole-3-acetic-acid but not of 2,4-dichlorophenoxyacetic acid, an auxin analog that is not recognized by the polar transport machinery, and accumulation of the auxin transporter PIN-FORMED1 (PIN1) was sensitive to calcium levels in the *ro/big* mutants. Consistent with a role for calcium in mediating auxin transport, both *ro/big* mutants and calcium-treated wild-type plants were hypersensitive to treatment with polar auxin transport inhibitors. Subcellular localization of BIG suggests that, like its mammalian ortholog, it is associated with the endoplasmic reticulum. Analysis of subcellular morphology revealed that *ro/big* mutants exhibited disruption in cytoplasmic streaming. We suggest that RO/BIG maintains auxin flow by stabilizing PIN membrane localization, possibly by attenuating the inhibitory effect of Ca^{2+} on cytoplasmic streaming.

Keywords: *Arabidopsis* ● Auxin transport ● BIG ● Calcium ● Tomato ● UBR4 ● Wound-induced roots

Editor-in-Chief's Choice

Introduction

Plants can recover from loss or damage to their root system by producing new roots from their shoots and hypocotyls. These roots are generally referred to as adventitious roots (ARs), but in specific developmental contexts, these are called shoot-borne roots (SBRs), and when formed in response to injury, these are called wound-induced roots (WiRs). WiR initiation is regulated by a range of phytohormones which play a role in all stages of root formation (Bellini et al. 2014, Steffens and Rasmussen 2016, Omary et al. 2022).

Auxin [indole-3-acetic acid (IAA)] is the central hormone controlling WiR initiation (Pacurar et al. 2014), and increased levels of endogenous or exogenous auxin promote root formation in many plant species, a property commonly utilized for clonal propagation (Boerjan et al. 1995, Delarue et al. 1998, de Klerk et al. 1999, Druege et al. 2016, Lakehal and Bellini 2019, Guan et al. 2019). The transcriptional response to auxin is mediated by AUXIN RESPONSE FACTOR transcription factors which, in the presence of auxin, are released from their inhibitors, AUX/IAAs, and allowed to bind auxin response elements in promoters of target genes (Weijers and Wagner 2016). Consistent with auxin's role in WiR initiation, the synthetic auxin-responsive promoter DR5 (Ulmasov et al. 1997) is induced at the earliest stages of WiR initiation (Welander et al. 2014, Della Rovere et al. 2016).

Auxin distribution within tissues is determined both by its site of biosynthesis and by the activity of polar and nonpolar auxin transporters. Auxin is produced from the amino acid tryptophan by the enzymes TRYPTOPHAN AMINOTRANSFERASE OF ARABIDOPSIS and YUCCA (Zhao 2014). The cellular uptake of auxin is mediated by the AUXIN-RESISTANT1 (AUX1)/LIKE AUX1 family of nonpolar transporters (Swarup and Péret 2012), while its export is mainly controlled by the PIN-FORMED transporters (PINs), which are polarly localized on the plasma membrane (PM) (Adamowski and Friml 2015). While most PINs are localized to the PM, the *Arabidopsis* (*Arabidopsis thaliana*) PIN5, PIN6 and PIN8 were shown to also localize to the endoplasmic reticulum (ER) membrane, where they regulate intracellular auxin distributions together with PIN-LIKE

Plant Cell Physiol. 64(2): 152–164 (2023) doi:https://doi.org/10.1093/pcp/pcac163, Advance Access publication on 18 November 2022, available online at https://academic.oup.com/pcp

proteins (Adamowski and Friml 2015, Simon et al. 2016, Sauer and Kleine-Vehn 2019).

The PINs are required for directional auxin transport within plant tissues, and disruption of their activity, either genetically or using the chemical inhibitor naphthylphthalamic acid (NPA), results in altered auxin distribution within tissues (Sabatini et al. 1999, Adamowski and Friml 2015, Abas et al. 2021). NPA blocks IAA transport by directly binding the PIN proteins (Abas et al. 2021, Teale et al. 2021, Ung et al. 2022), but other possible NPA targets were suggested, such as ATP-binding cassette transporters or their interacting partner TWISTED DWARF (Teale and Palme 2018). An early putative NPA target is the large callosin-like protein BIG/TRANSPORT INHIBITOR RESPONSE 3 (TIR3), which plays a role in the regulation of the auxin transport. *big* mutants are characterized by reduced auxin transport rates, reduced binding of NPA and reduced levels of PIN proteins (Ruegger et al. 1997, Gil et al. 2001, Liu et al. 2022).

How endogenous auxin gets to the initiating WiR is not entirely known. Mutants defective in auxin import or PIN-mediated auxin export have reduced the number of WiRs (Sukumar et al. 2013, Lee et al. 2019), and using local application of NPA to block auxin transport from the shoot results in a reduction in the number of formed roots. This suggests that most of the auxin required for WiR formation is shoot-derived (Ahkami et al. 2013, Sukumar et al. 2013, Alaguero-Cordovilla et al. 2021).

Apart from hormones, other molecules also mediate WiR initiation. Among these, Ca^{2+} is a universal secondary messenger involved in many cellular processes, including auxin signaling (Dodd et al. 2010, Vanneste and Friml 2013). Ca^{2+} can be sensed by calmodulin (CaM), a small protein that regulates the activity of other proteins by interacting with their CaM-binding domain (Dodd et al. 2010). The effects of Ca^{2+} levels on WiR initiation are complex and were mainly studied in tissue culture conditions. Ca^{2+} treatment can enhance the root-promoting effect of IAA in poplar (Bellamine et al. 1998) and mung bean (*Phaseolus aureus*) when applied together with borate (Jarvis and Yasmin 1985) but had no effect in *Dalbergia* (Ansari and Kumar 1994). Chelating Ca^{2+} using EGTA partially inhibited adventitious rooting in poplar and mung bean (Bellamine et al. 1998, Li and Xue 2010), but a transient EGTA treatment promoted rooting in sunflower (Kalra and Bhatia 1998). In cucumber, inhibition of CaM activity counteracted the root-promoting effects of exogenous auxin or nitric oxide (Lanteri et al. 2006, Niu et al. 2017), and the application of Ca^{2+} activated ethylene signaling to relieve the repression of rooting promoted by salt stress (Yu et al. 2019). In mung bean, it was suggested that Ca^{2+} acts downstream of auxin, H_2O_2 and nitric oxide (Lanteri et al. 2006, Li and Xue 2010). Overall, how Ca^{2+} and auxin interact during WiR initiation is still unclear.

Tomato (*Solanum lycopersicum*) has been used as a model species for developmental studies of both shoot and root systems and recently also as a model for WiR formation (Alaguero-Cordovilla et al. 2021). Several mutations that affect SBR production in tomato were identified, which serve as promising candidates for WiR regulators (Zobel 1975). The classical tomato mutation *rosette* (*ro*) displays a severe reduction in internode elongation, reduced branching and complete sterility. Notably, these plants were described to have no SBR and a reduced number of lateral roots (LRs; Butler 1954, Zobel 1975, Schiefeibein et al. 1991). Although first described in 1954, the causal mutation underlying the *ro* phenotype was never identified. Here, we show that *ro* mutants are defective in WiR initiation. We map *ro* to the tomato ortholog of *BIG* and show that the reduction in WiR formation in these mutants is likely attributed to Ca^{2+}-related disruption of the polar auxin transport machinery. Finally, we show that RO/BIG is likely localized to the ER and is important for maintaining proper cytoplasmic streaming, suggesting a possible link between subcellular organization and tissue-wide auxin distribution patterns.

Results

ro is defective in WiR production and auxin transport

Tomato *ro* mutants are dwarf and exhibit little internode elongation, and their stems and hypocotyls are narrow compared to wild-type (WT) plants (**Fig. 1A–C**; Butler 1954). Dissection of the hypocotyl of 4-week-old plants revealed that both the WT and *ro* mutants had a similar organization with four opposing vascular bundles. The width of the cortex was reduced by 30% in the *ro* mutant (WT $578 \pm 7.6\,\mu m$, *ro* $403 \pm 10.2\,\mu m$; $n = 8$; $P < 0.0001$; Student's *t*-test), but most of the reduction in stem width was due to a 75% reduction in stele width (WT $2123 \pm 198\,\mu m$, *ro* $528 \pm 28\,\mu m$; $n = 8$; $P < 0.0001$; Student's *t*-test). Additionally, *ro* mutants lacked interfascicular cambium (**Fig. 1D–F**). As previously reported, uninjured *ro* plants produced no SBR from their hypocotyls (Schiefeibein et al. 1991; **Fig. 1G, H**). To test whether the *ro* mutation also affects WiR production, we removed the root system of 4-week-old *ro* plants and WT siblings and allowed the cuttings to root in deionized water. After 10 d, WT plants formed a large number of roots all along the hypocotyl, while *ro* cuttings formed only a few roots at the base of the hypocotyl (WT 54 ± 13, *ro* 5.1 ± 2.8 roots per plant; $n = 20$; $P < 0.0001$; Student's *t*-test; **Fig. 1I, J**).

To test whether exogenous auxin can rescue the *ro* WiR phenotype, we treated cuttings with 10 μM IAA. As previously reported (Alaguero-Cordovilla et al. 2021), this treatment increased the number of roots in WT plants. While IAA also increased the number of WiRs in *ro* plants, the response was attenuated, the number of roots remained low and they were confined to the bottom of the hypocotyl, near the cut site (**Fig. 1K–N**). We further evaluated whether auxin-induced *de novo* root formation was affected by the *ro* mutation using young cotyledon explants. When tomato cotyledons are dissected and placed on agar media containing the synthetic auxin naphthylacetic acid (NAA), they can produce AR. *ro* mutants developed fewer roots that produced fewer LR than WT (**Fig. 1O–R**).

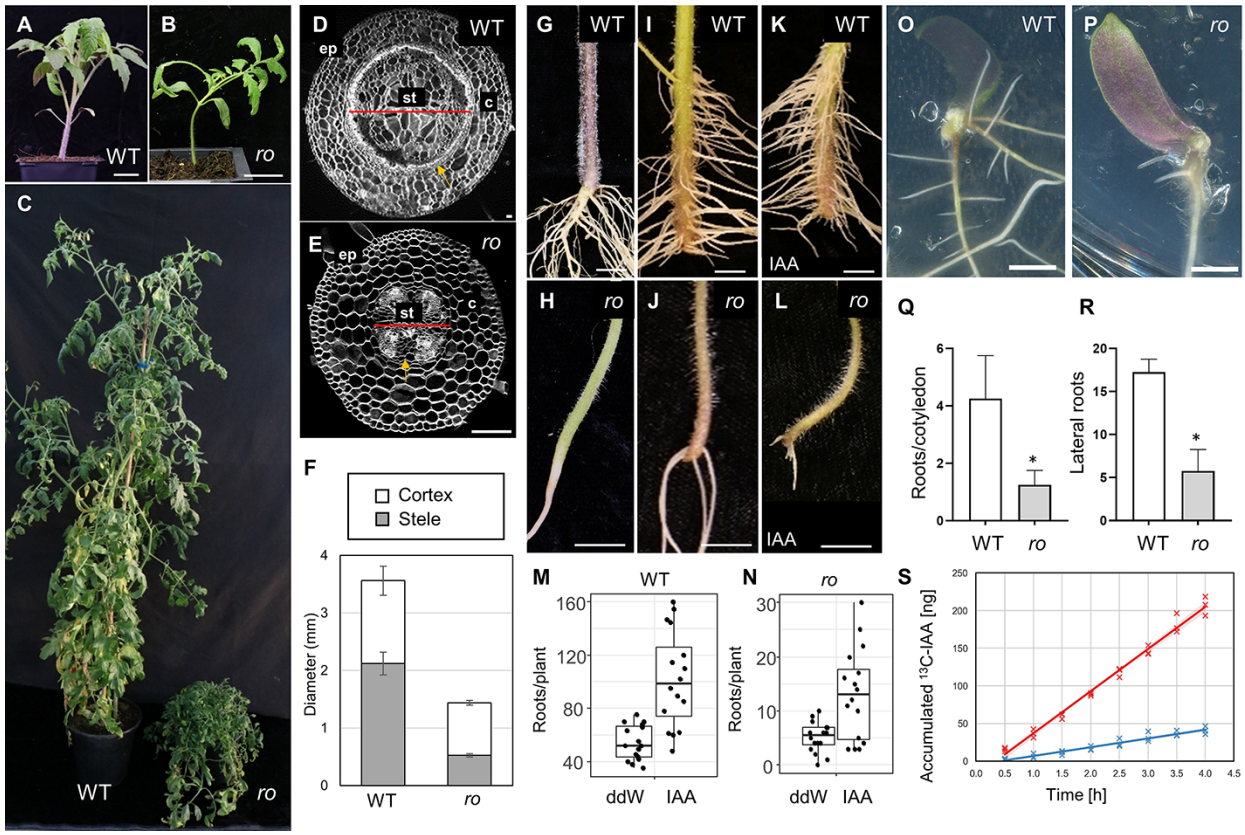

Fig. 1 The classical *ro* mutation is defective in WiR production. (A–C) Tomato WT and *ro* 1-month-old (A, B) and 5-month-old (C) plants. (D, E) Confocal images of hypocotyl cross-sections of WT (D) and *ro* (E). Cell wall was stained with SCRI Renaissance 2200. Note that the WT and *ro* panels are at different scales. ep—epidermis; st—stele; c—cortex. Central line marks the diameter of the stele. Arrows point to the interfascicular cambium in (D) and its absence in (E). (F) Diameters of entire hypocotyl and its stele in WT and *ro* mutants ($n = 8$ for WT and *ro*). (G, H) Close-up images of hypocotyls of WT (G) and *ro* (H). (I–L) WiR in hypocotyls production 10 d after cutting (dac) in WT (I, K) and *ro* (J, L), either when incubated in water (I, J) or with 10 μM IAA (K, L). (M, N) Quantification of WiR production in WT (M) and *ro* (N) cuttings incubated in water or 10 μM IAA. The bar indicates the mean. Two-tailed Student's *t*-test: WT-ddW vs IAA, $P < 0.01$ ($n = 20$ and 20 for ddW and IAA, respectively); *ro*-ddW vs IAA, $P < 0.01$ ($n = 20$ and 20 for ddW and IAA, respectively). (O, P) Cut cotyledons of 7–8-day-old WT (O) and *ro* (P) plants incubated on TK4 media with 50 nM NAA for 12 d. (Q, R) Quantification of WiR (Q) and LR (R) numbers formed on cotyledons ($n = 4$ for each condition; $P < 0.01$, two-tailed Student's *t*-test). (S) Accumulated transported IAA in WT and *ro* tomato hypocotyls. $n = 3$ for each genotype. Scale bars are 1 cm in (A, B, G–L, O, P) and 100 μm in (D, E).

Previously, it was shown that inhibition of auxin transport rates using NPA reduced the number of roots formed on cut tomato hypocotyl (Alaguero-Cordovilla et al. 2021). To test whether auxin transport rates are affected in *ro*, we applied radiolabeled IAA to the apical side of hypocotyl sections of WT and *ro* mutants and detected its accumulation in the basal side. We found that IAA transport intensity through the hypocotyl was significantly reduced in *ro* mutants, with a 5-fold difference in IAA transport rates compared to WT (**Fig. 1S**; 56.03 ± 3.61 ng h^{-1} in WT and 11.64 ± 0.97 ng h^{-1} in *ro* mutants; $P < 0.001$; Student's *t*-test). Overall, our results suggest that *ro* is disrupted in the formation of WiRs, possibly due to the inability to form sufficient auxin concentrations at the hypocotyl/cotyledon base.

ro is a mutation in the tomato ortholog of *BIG*

To better understand the role of *RO* in WiR initiation, we turned to mapping-by-sequencing to identify the causal mutation. Previous genetic linkage experiments have mapped *ro* to the long arm of chromosome 2 in a linkage group with *dwarf* (*Solyc02g089160*; Butler 1954). We e-sequenced a pool of 12 *ro* mutant plants and 12 WT-looking siblings to a coverage of 40×. We identified a region of homozygosity in the *ro* mutant pool on chromosome 2 between 50,475,714 and 51,141,636 bp (ITAG2.5 coordinates). This region contained 88 genes, including the *DWARF* locus. Only one mutation that disrupted the amino acid sequence was identified in this region; a transversion causing a premature stop at the eighth exon of *Solyc02g089260* (11725A>T; **Fig. 2A**; **Supplementary Fig. S1A, B**). To confirm that the *ro* mutant is caused by a disruption to *Solyc02g089260*, we generated clustered regularly interspaced short palindromic repeat (CRISPR)-edited plants of this gene in tomato M82 background. A CRISPR-induced insertion at the third exon caused an early frameshift, likely resulting in a null allele (**Fig. 2A**; **Supplementary Fig. S1A**). Like *ro*, these mutants had no internode elongation, their leaves were small and simple and they

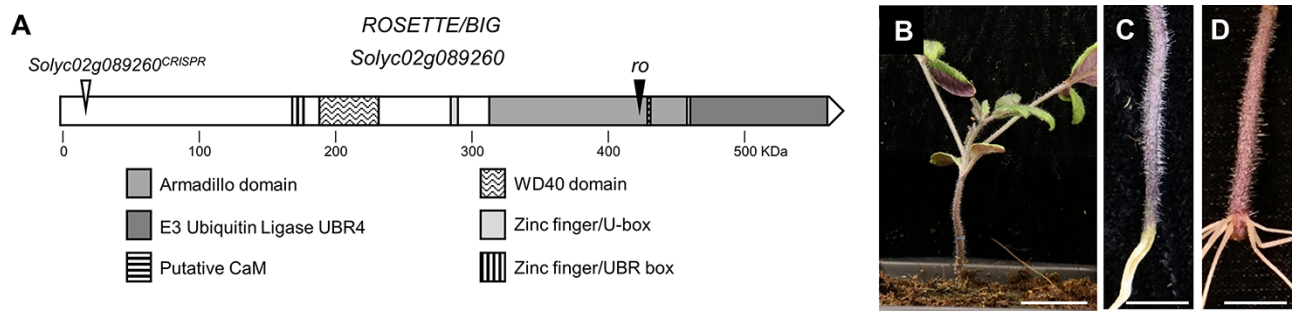

Fig. 2 *ro* maps to the tomato ortholog of *BIG*. (A) Schematic representation of the *RO/BIG* protein. White and black triangles indicate the position of the tomato *Solyc02g089260*^{CRISPR} and the *ro* mutations, respectively. (B–D) One-month-old *Solyc02g089260*^{CRISPR} mutant plant (B) with no SBR (C) but with WiR on cut hypocotyls (D). Scale bars are 5 cm in (B) and 2 cm (C, D).

lacked SBR. As in *ro* plants, *Solyc02g089260*^{CRISPR} mutants could form a few WiRs when the root system was removed, but those were confined to the base of the hypocotyl (**Fig. 2B–D**). To confirm that the *ro* phenotype is caused by disruption of *Solyc02g089260*, we performed an allelism test and crossed *ro*/+ with *Solyc02g089260*^{CRISPR}/+ plants. About one-fourth of the F1 progeny had the *ro* phenotype, indicating that *ro* is allelic to *Solyc02g089260*^{CRISPR} and is likely also a null allele (**Supplementary Fig. S1D**).

Solyc02g089260 is a very large protein (5104 aa) with no duplicated family members. Its closest ortholog in *Arabidopsis* is BIG (AT3G02260), and that in mammalians is UBR4/p600 (Gil et al. 2001, Nakatani et al. 2005). Domain annotation using Expasy identified several Zinc fingers, WD40, armadillo and E3-ubiquitin ligase domains. Previous work has shown that BIG also has a noncanonical CaM-binding domain (Belzil et al. 2013). These domains in *Solyc02g089260* were similar in identity and position to the *Arabidopsis* BIG, indicating that RO, BIG and UBR4 are likely orthologs (**Fig. 2A**).

In *Arabidopsis, BIG* was reported to be important for a variety of developmental and physiological processes, such as regulation of light and shade responses, circadian rhythms, gibberellin status and both root and shoot development (Gil et al. 2001, Kanyuka et al. 2003, Desgagné-Penix et al. 2005, Hearn et al. 2018, Liu et al. 2022). To determine whether *BIG* plays a similar role in WiR initiation in *Arabidopsis* as it does in tomato, we dissected the root system of 5-day-old WT and plants carrying the *tir3-1* allele (which we refer to hereafter as *big*; **Supplementary Fig. S1A, E**; Ruegger et al. 1997). Consistent with the *ro* phenotype, the number of WiRs in *big* seedlings was significantly reduced, and they took longer to appear (**Fig. 3A–C**). Treatment with IAA increased the number of WiRs forming on both WT and *big* hypocotyls (Gutierrez et al. 2009), but the number of roots was lower than in comparably treated WT plants (**Fig. 3D**).

To determine whether root initiation or emergence was defective in *big*, we examined the dynamics of the auxin reporter *DR5rev:3xVENUS-N7*, which marks the early stages of WiR initiation in the hypocotyl (Welander et al. 2014). In WT *Arabidopsis*, auxin signaling was induced at the bottom of the hypocotyl at 6 h after the cut, and focused signals marking root primordia were apparent at 24 h. Auxin signaling was attenuated in *big* mutants and was apparent near the cut site by 24 h, while primordia were observed only at 48–72 h (**Fig. 3E**). This 24-h delay in induction of the auxin response in *big*, as compared to WT, is consistent with a similar 24-h delay in the appearance of the roots (**Fig. 3C**). This suggests that *big* is inhibited in initiation, rather than emergence, of the WiR and is consistent with inhibition of auxin transport being responsible, at least in part, to the *big* root initiation phenotype.

Ro/big mutants are hypersensitive to Ca^{2+} in WiR formation

The application of exogenous auxin could not fully rescue *big* root initiation defects (Liu et al. 2022), prompting us to identify other factors that could be defective in *big*. The plant and mammalian *RO/BIG/UBR4* genes have a CaM-binding domain. It was suggested that *UBR4*'s function is to protect the integrity of subcellular organelles from increased Ca^{2+} levels during neuronal Ca^{2+} spikes (Belzil et al. 2013). In *Arabidopsis*, *big* mutants were reported to have increased cytosolic Ca^{2+} accumulation in seedling leaves (Hearn et al. 2018), suggesting that it may be involved in Ca^{2+} homeostasis. As it was previously reported that Ca^{2+} levels could affect WiR initiation rates (Lanteri et al. 2006, Yu et al. 2019), we tested whether altered Ca^{2+} response may underlie some of the root initiation defects in tomato *ro* and *Arabidopsis big*.

Treatment of tomato cuttings with 2 mM Ca^{2+} did not affect WT control plants but inhibited WiR production in *ro* (**Fig. 4A, B**). Chelating the Ca^{2+} with EGTA restored root production (**Fig. 4C, D**), while the $MgCl_2$ control treatment did not affect either WT or *ro* (**Fig. 4E, F**).

To test whether the sensitivity to calcium is a conserved trait of *ro/big* mutants, we tested the formation of WiRs in *Arabidopsis* under mock conditions (no Ca^{2+}) and with increasing concentrations of Ca^{2+}. The number of hypocotyl WiRs was not affected by exogenous Ca^{2+} in WT *Arabidopsis* but was reduced in a dose-dependent manner in *big* mutants, suggesting that these mutants were sensitive to calcium also in

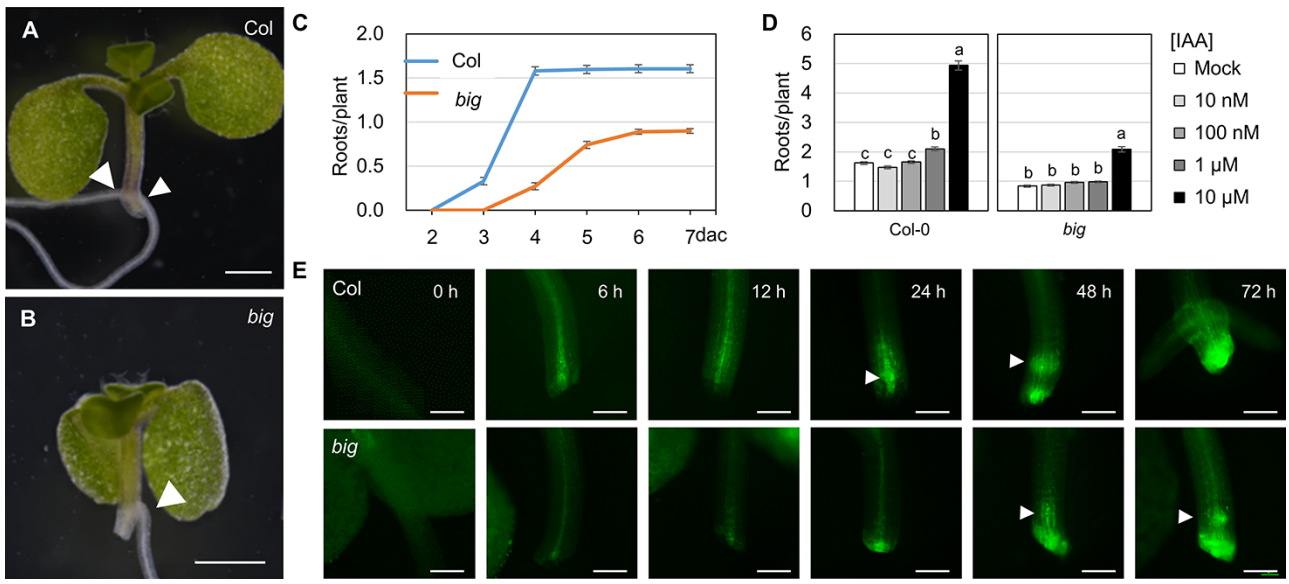

Fig. 3 *Arabidopsis big* mutants are defective in WiR initiation. (A, B) *Arabidopsis* Col WT (A) and *big* (B) mutants 7 dac of the root system. Arrowheads mark root primordia. (C) WiR production in Col and *big* cuttings incubated in water ($P < 0.01$, $n = 124$ and 128 for Col and *big*, respectively). (D) Number of WiRs in *Arabidopsis* Col and *big* mutant cuttings after 7 d treated with different IAA concentrations ($n = 125$, 132, 127, 135 and 138 for Col and 137, 130, 131, 137 and 143 for *big* in mock, 10, 100 nM, 1 and 10 µM IAA, respectively). Bars represent the mean ± SE; letters are statistically significant differences ($P < 0.01$; ANOVA and Tukey's post hoc test). (E) Stereomicroscope images of *DR5rev:3xVENUS-N7* cuttings in Col (upper panels) and *big* (lower panels) backgrounds. Arrowheads mark root primordia. At least six plants were examined, and representative images were shown. Scale bars are 1 cm (A) and 200 µm (E). ANOVA, analysis of variance.

Arabidopsis (**Fig. 5A**). We note that higher concentrations of Ca^{2+} were required to observe an effect in *Arabidopsis*, compared to tomato. Treatment with $MgCl_2$ had the same effect on both WT and *big* mutants, suggesting that the hypersensitivity of the mutant is specific to Ca^{2+} (**Fig. 5B**). Consistently, a high level of Ca^{2+} had no effect on the *DR5rev:3xVenus-N7* signal in WT plants but delayed the appearance of the signal in *Arabidopsis big* mutants, where DR5 activation was not apparent even at 72 h after the cut (**Fig. 5C** and compare to **Fig. 3E**). Overall, these results are consistent with altered Ca^{2+} levels interfering with auxin transport in *ro*/*big* mutants.

Ca^{2+} increases plant sensitivity to auxin transport inhibition

To determine whether the inhibitory effect of Ca^{2+} on WiR stems from a defect in the transport machinery, we co-treated WT and *big* plants with Ca^{2+} and IAA. The addition of 10 mM Ca^{2+}, which by itself had little-to-no effect on root production in both WT and *big*, resulted in suppression of IAA-promoting effect on root number (**Fig. 6A**). Treatment with the synthetic auxin 2,4-dichlorophenoxyacetic acid (2,4-D), which is not carried by the PIN proteins (Yang and Murphy 2009), increased root production in both WT and *big* mutant cuttings but was not sensitive to calcium treatment. Moreover, 2,4-D had a significantly stronger effect on *big* mutants, increasing the number of roots 3.3-fold compared to the 1.7-fold increase produced by IAA (**Fig. 6B**).

If Ca^{2+} mediates its effect on root production by disrupting auxin transport, we can expect calcium treatment to act synergically with NPA and that *big* mutants would be sensitive to inhibition of auxin transport. In WT, treatment with 1 µM NPA resulted in a 23% reduction in root formation, while applying 10 µM NPA almost completely inhibited root initiation (96% reduction). *big* mutants were hypersensitive to NPA, and a 46% reduction in root number was apparent already at 100 nM NPA. Unlike WT plants, 1 µM NPA was sufficient to block root initiation in big (**Fig. 6C**) completely. NPA treatment prevented the activation of an auxin response signal near the cut in *big*, which is correlated with the lack of root initiation (**Fig. 6D**).

As expected from our hypothesis, treating cuttings with $CaCl_2$ resulted in hypersensitivity to NPA. When $CaCl_2$ was present in the media, WT plants exhibited a reduced WiR number already at 100 nM NPA, and root production was abolished at 1 µM NPA, a response profile that phenocopied the response of *big* to NPA (**Fig. 6C, E**). Media containing calcium aggravated the response of *big* mutants to NPA (**Fig. 6F**). We note that *big* mutants were initially identified due to their resistance to NPA treatment in a primary root growth assay (Ruegger et al. 1997). The apparent contradiction between this and the NPA sensitivity shown here is probably due to the differences in development contexts (Gil et al. 2001).

Indeed, it was previously reported that NPA could induce the internalization of PIN proteins in *big* mutants but not in WT (Gil et al. 2001). Furthermore, levels of PM-PINs in the root meristem were reduced in *big* mutants (Liu et al. 2022).

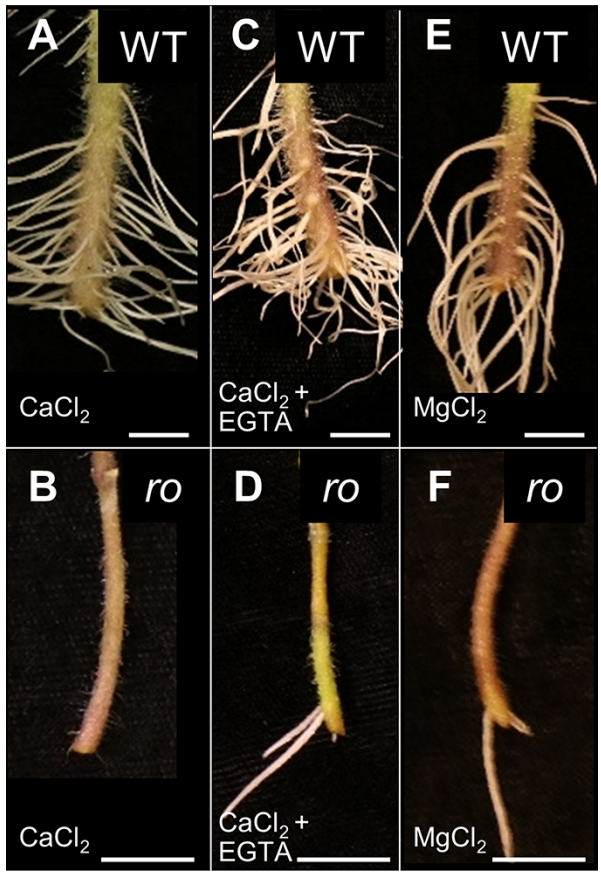

Fig. 4 Root initiation in the tomato *ro* mutant is sensitive to exogenous Ca^{2+}. (A–F) One-month-old WT (A, C, E) or *ro* (B, D, F) tomato cuttings incubated in 2 mM $CaCl_2$ (A, B), 2 mM $CaCl_2$ + 2 mM EGTA (C, D) and 500 μM $MgCl_2$ (E, F) for 7 d. Scale bars are 1 cm.

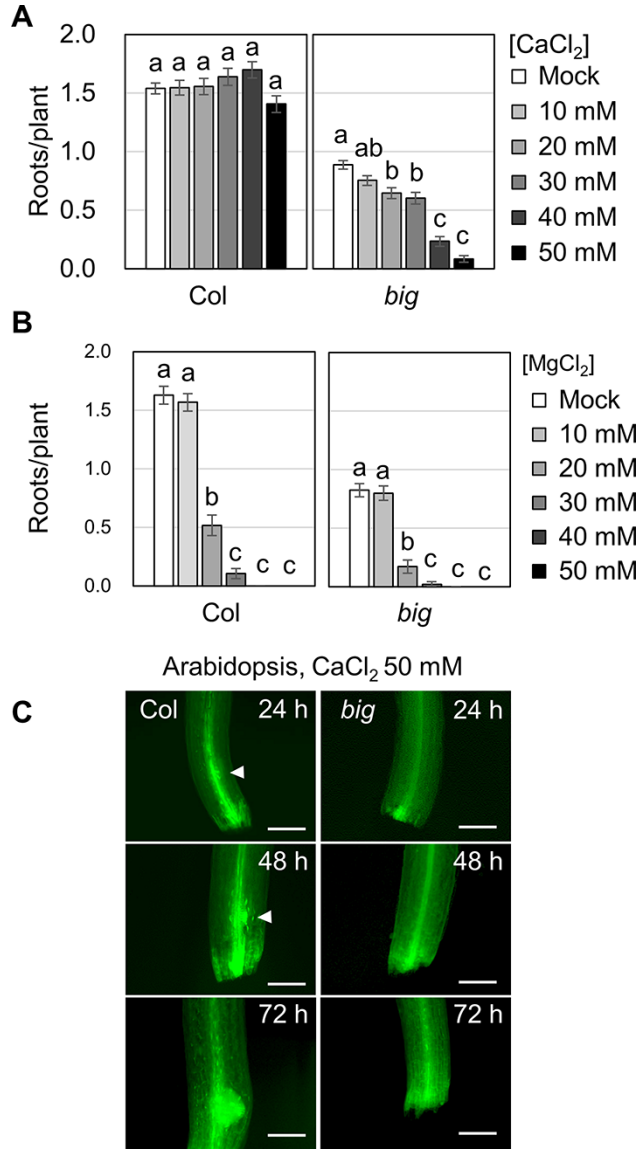

Fig. 5 *Arabidopsis big* mutants are sensitive to exogenous Ca^{2+}. (A, B) Number of WiRs in *Arabidopsis* WT Col and *big* mutant cuttings at 7 dac treated with different concentrations of $CaCl_2$ (A) or $MgCl_2$ (B) ($n = 124$, 106, 120, 114, 116 and 113 for Col and 89, 102, 116, 106, 106 and 105 for *big* in mock, 10, 20, 30, 40 and 50 mM $CaCl_2$, respectively; $n = 108$, 112, 107, 121, 116 and 112 for Col and 91, 86, 96, 93, 103 and 104 *big* in mock, 10, 20, 30, 40 and 50 mM $MgCl_2$, respectively). (C) Stereo microscope images of *DR5rev:3xVENUS-N7* cuttings incubated in 50 mM $CaCl_2$ in Col (left) and *big* (right) backgrounds. Arrowheads mark root primordia. At least six plants were examined, and representative images were shown. Bars represent the mean ± SE; letters are statistically significant differences ($P < 0.01$; ANOVA and Tukey's post hoc test). Scale bars are 200 μm. ANOVA, analysis of variance.

We, therefore, tested whether the Ca^{2+} treatment could also affect PIN1 accumulation by using immunohistochemistry in the tomato root meristem. Supporting the link between Ca^{2+} and PIN localization, calcium depletion caused a reduction of *PIN1* immunostaining signal in the tomato root meristem. This reduction was much more pronounced in *ro* mutants (**Fig. 6G–K**). We note that in the root meristem, we observed a differential effect in low levels of exogenous Ca^{2+}, while the phenotypic effect on root initiation was apparent at high Ca^{2+} levels. While we do not have a clear explanation for this discrepancy, the differential response suggests that these mutants are more sensitive to changes in Ca^{2+} levels than WT.

The auxin transport system is composed of PM and ER-bound PINs (Sauer and Kleine-Vehn 2019), and both types were suggested to play a part in WiR (Xu et al. 2005, Simon et al. 2016, da Costa et al. 2020). To determine which PIN family plays the major role in WiR production, we tested WiR formation in single and high-order *pin* mutants. The effect of mutants in ER-localized PINs was low, and changes in the number of roots were only significant in the *pin5* mutant, with a mild 15% reduction in our experimental system. No aggravation of this phenotype was observed when all three ER-localized PINs were mutated, and their response was not significantly different from WT plants (**Fig. 6L**). In contrast, PM-PINs were required for root initiation, with *pin1;2* mutants exhibiting a 32% reduction in rooting rates and the quintuple mutant *pin1;2;3;4;7* not forming roots at all (**Fig. 6M**), indicating that the PM-PINs are the

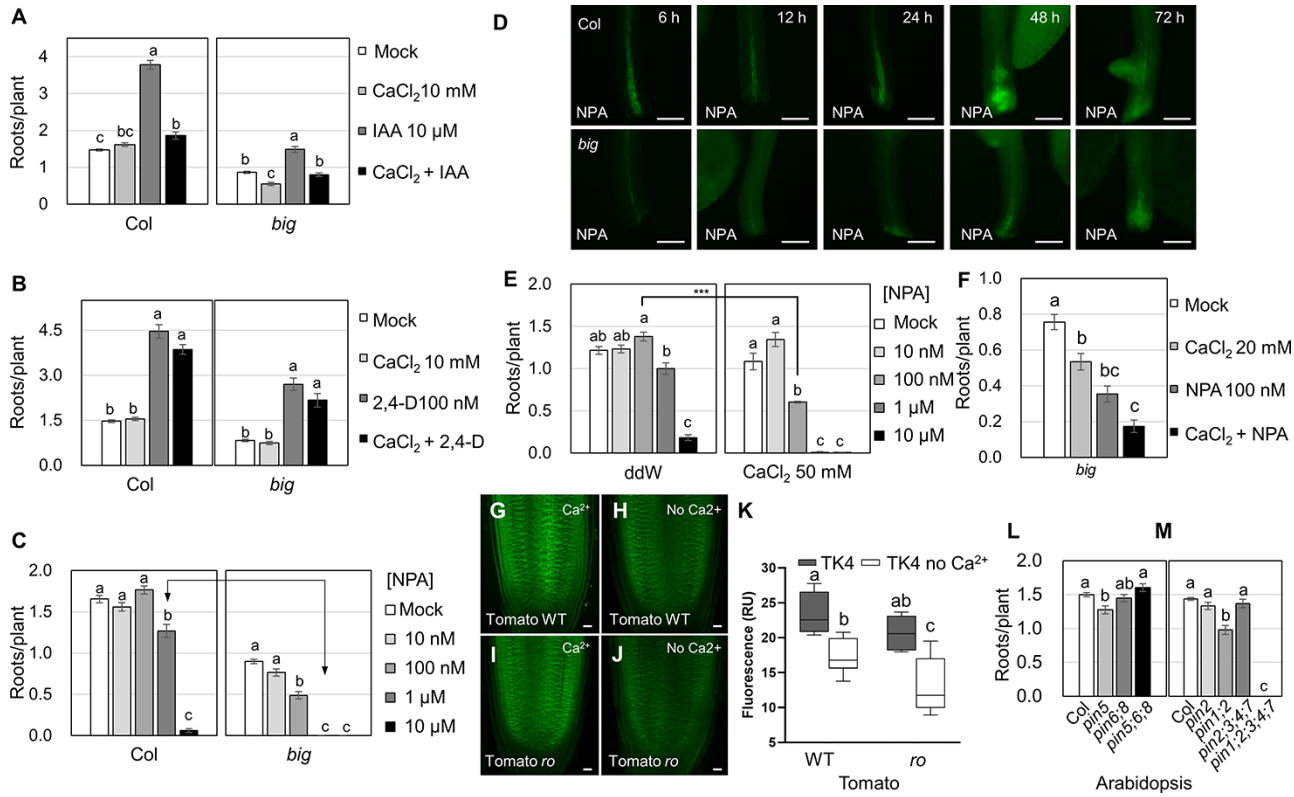

Fig. 6 Altered Ca^{2+} levels control root initiation by inhibition of polar auxin transport. (A–C) WiR rates in 7 dac Col and *big* in different treatments ($n = 125$, 127, 133 and 130 for Col and 129, 129, 127 and 134 for *big* in mock, 10 mM $CaCl_2$, 10 µM IAA and 10 mM $CaCl_2$ + 10 µM IAA, respectively; $n = 120$, 123, 108 and 115 for Col and 101, 94, 67 and 70 for *big* in mock, 10 mM $CaCl_2$, 100 nM 2,4-D and 10 mM $CaCl_2$ + 100 nM 2,4-D, respectively; $n = 119$, 110, 124, 130 and 114 for Col and 119, 98, 131, 127 and 133 for *big* in mock, 10, 100 nM, 1 and 10 µM NPA, respectively). (D) Stereo microscope images of *DR5rev:3xVENUS-N7* cuttings incubated in 100 nM NPA in WT (upper panels) and *big* (bottom panels) backgrounds. (E, F) Number of WiRs in WT (E) and *big* (F) plants cotreated with NPA and $CaCl_2$ for 7 d (WT, $n = 116$, 121, 129, 130 and 126 for no Ca^{2+} and 119, 119, 111, 115 and 111 for Ca^{2+} containing media in mock, 10, 100 nM, 1 and 10 µM NPA, respectively; *big*, $n = 119$, 116, 113 and 121 for mock, 20 mM $CaCl_2$, 100 nM NPA and 20 mM $CaCl_2$ + 100 nM NPA, respectively). (G–J) Confocal images of WT (G, H) and *ro* (I, J) tomato root meristems after 18-h incubation with TK4 media (G, I) and calcium-free TK4 media (H, J). (K) Quantification of fluorescence signals in (G–J), $n = 4$. (L, M) Number of WiRs in mutants of ER-PINs (L) and PM-PINs (M) at 7 dac ($n = 317$, 98, 108 and 125 for Col, *pin5*, *pin6*;8 and *pin5*;*6*;*8*, respectively; $n = 303$, 84, 45, 106 and 84 for Col, *pin2*, *pin1*;2, *pin2*;*3*;*4*;*7* and *pin1*;*2*;*3*;*4*;*7*, respectively). Bars represent the mean ± SE; letters are statistically significant differences ($P < 0.01$; ANOVA and Tukey's post hoc test) and asterisks are statistically significant differences by two-tailed Student's *t*-test (n.s., not significant, ***$P < 0.001$). Scale bars are 200 µm in (D) and 20 µm (G–J). ANOVA, analysis of variance.

ones playing the major role in the regulation of WiR initiation in the *Arabidopsis* hypocotyl.

Taken together, these results suggest that in *ro*/*big* mutants, Ca^{2+} levels interact with polar auxin transport, possibly by disrupting PM-PIN localization and preventing the auxin flow required for WiR initiation.

BIG has ER localization signals and is required for maintaining cytoplasmic streaming

It is unclear how *RO*/*BIG* could control PIN activity since not much is known about the molecular function of this protein. In mammalians, UBR4/p600 was suggested to be localized to the ER, where it maintains ER integrity under high Ca^{2+} conditions (Shim et al. 2008, Belzil et al. 2013). To test whether such a function may be conserved in plants, we first tested the intracellular localization of BIG. BIG is a 570-kDa protein, and we could not construct a complete protein fusion. We, therefore, opted to generate partial protein fusions. We fused six parts of the protein to mScarlet-i and transiently expressed them in *Arabidopsis* cotyledons (**Supplementary Table S1**). Fusions for five of the six parts of the proteins did not produce any signal, suggesting that these are unstable. However, a fusion of the 251-aa C-terminal region resulted in ER localization, which was verified by co-localizing with the ER marker yellow fluorescent protein (YFP)–His-Asp-Glu-Leu (HDEL) (**Fig. 7A–C**).

To test whether BIG plays a role in maintaining the structure of intracellular organelles, we examined the morphology of the ER in *big* mutants using the ER-localized makers YFP–HDEL (Saint-Jore-Dupas et al. 2006, Nelson et al. 2007). Examination of cotyledon epidermal cells revealed no obvious structural disruption to the ER (**Fig. 7D, E**). However, we could

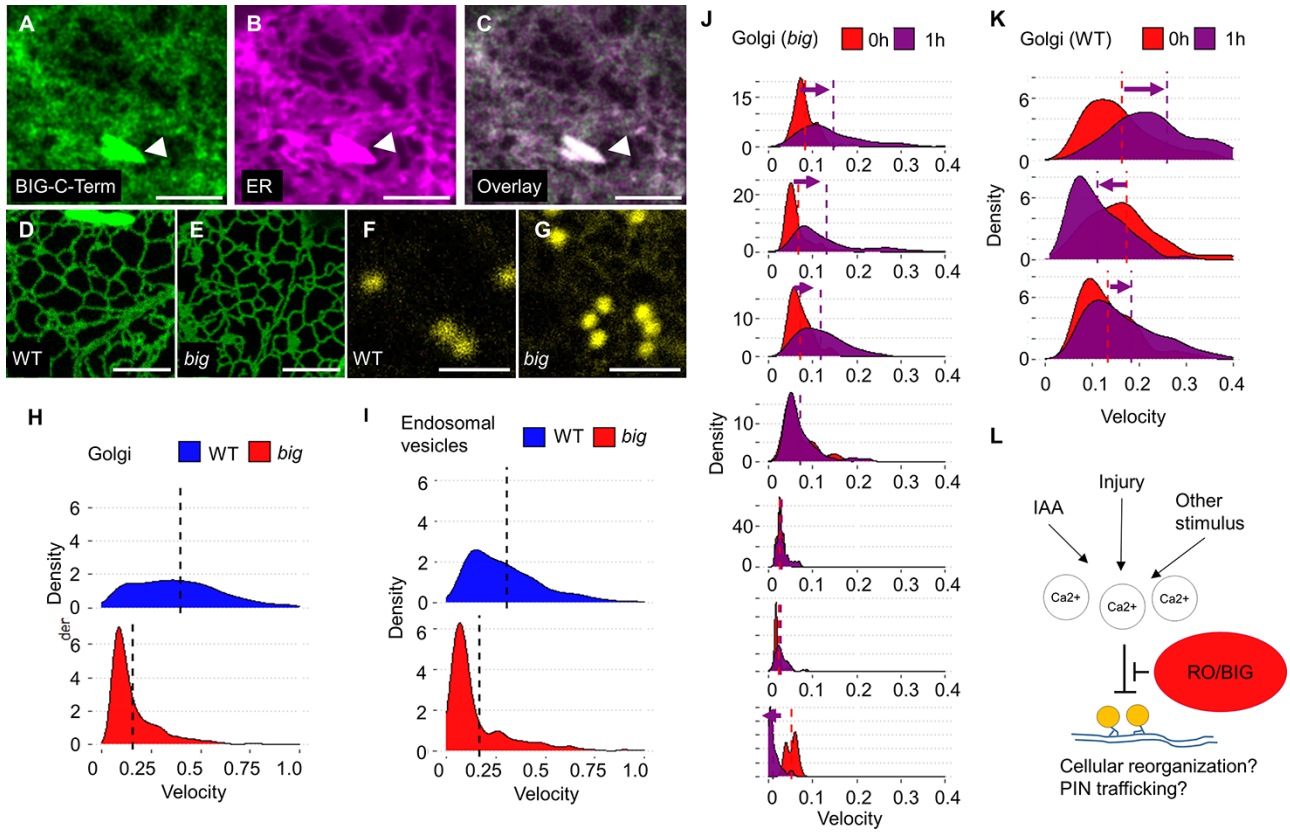

Fig. 7 BIG is associated with the ER and is required for maintaining subcellular movement. (A–C) Confocal images of the C-terminal region of the BIG protein fused to the mScarlet-i (A), the ER marker YFP–HDEL (B) and the overlay of both (C) in epidermal cells of *Arabidopsis* cotyledons. Arrowheads point to ER bodies. (D–G) Confocal images of the ER marker GFP-HDEL (D, E) and the Golgi marker Man49-YFP (F, G) in Col (D, F) and *big* (E, G) epidermal cells of *Arabidopsis* cotyledons. (H, I) Distribution of velocities of Golgi bodies (H) and endosomal vesicles (I) in Col and *big* mutant epidermal cells (Golgi: WT 0.4 ± 0.007 μm/s, *big* 0.16 ± 0.004 μm/s, $n = 1123$ and 954 for WT and *big*, respectively, $P < 0.0001$, Student's *t*-test; endosomal vesicles: WT 0.31 ± 0.009 μm/s, *big* 0.17 ± 0.008 μm/s, $n = 540$ and 630 for WT and *big*, respectively, $P < 0.0001$, Student's *t*-test). (J–K) Distribution of velocities of Golgi bodies in individual epidermal cells of *big* (J) and WT control (K) at time 0 and 1 h later. Each distribution plot represents a single cell observed at the two time points (arrows mark a significant change in the mean velocity between the time points, $P < 0.0001$ in Student's *t*-test); dash lines indicate the mean velocity. (L) Hypothetical model for the function of RO/BIG. Scale bars are 5 μm.

observe abnormal inhibition of ER movement in cells of *big* mutants. To quantify this effect, we used the Golgi marker Man49, as the Golgi is tethered to the ER and its punctate nature makes them easy to track (Sparkes et al. 2009). As evidenced by the Man49 marker, Golgi morphology appeared normal in *big* (**Fig. 7F, G**). Time-lapse imaging of the Golgi in epidermal cells revealed a marked reduction in the average velocity of the Golgi organelle in the *Arabidopsis big* mutant. Notably, Golgi movement in 56% of the cells was almost wholly arrested (**Fig. 7H**).

The cytoplasm of plant cells continuously undergoes intracellular flow, promoted by the activity of myosin motors. This flow is arrested when cytosolic Ca^{2+} concentrations are elevated (Tominaga and Ito 2015) and enhanced in response to exogenous auxin (Friml et al. 2022). The observed arrest of Golgi and ER movement can be due to a specific effect on the ER or due to general arrest in cytoplasmic streaming and organelle movement. To distinguish between these possibilities, we measured the velocity of endosomal vesicles using the marker ARA6 (Ueda et al. 2001). The average velocity of endosomal vesicles was severely reduced in *big* mutants, to a similar extent as observed for the Golgi, with 53% of the cells exhibiting almost complete arrest of movement (**Fig. 7I**). To verify that this streaming arrest does not represent dead or dying cells, we performed a long-term time-lapse recording of the Golgi marker in *big* epidermal cells ($n = 7$), which appear arrested. One-hour-long recordings revealed that three out of the seven cells resumed Golgi movement (**Fig. 7J**), indicating that the arrest of organelle movement is transient and that cells can resume their activity. Similar changes in rates of Golgi streaming were observed in WT cells (**Fig. 7K**), but the arrest of streaming was rare. Taken together, our data suggest that *big* mutants are defective in organelle movement within the cell, a function linked to the regulation of cytoplasmic Ca^{2+} levels and short-term auxin response (Friml et al. 2022).

Discussion

Many plant developmental processes rely on the accumulation of auxin at specific places in the plant. In response to the cutting of the stem, changes in auxin transport and local biosynthesis lead to auxin accumulation near the wound site, promoting developmental responses to wounding, such as root initiation. Here, we show that the protein *RO/BIG* regulates auxin transport and accumulation in the context of wound response.

The phenotype of *RO/BIG* mutants is highly pleiotropic, but it was linked early on to the regulation of auxin transport (Ruegger et al. 1997, Gil et al. 2001, Kanyuka et al. 2003, Desgagné-Penix et al. 2005, Hearn et al. 2018, Liu et al. 2022). However, how *RO/BIG* affects auxin transport is not understood. We show that *ro/big* mutants are hypersensitive to exogenous Ca^{2+} levels in terms of PIN protein PM accumulation and the formation of a wound-induced auxin peak. Additionally, Ca^{2+} increased the sensitivity of both *ro/big* and WT plants to NPA. Together, this suggests that Ca^{2+} levels can affect the auxin transport machinery.

How does RO/BIG control auxin transport? At this point, we can only hypothesize. One possibility is that defects in ER organization may lead to disruption to the activity of ER-localized PINs. A previous study reported that mutants in the ER-localized *PIN6* have an increased rate of WiR (Simon et al. 2016). However, in our system, we could not observe any significant effect for the triple ER-PIN mutant *pin5;6;8* on WiR production. Rather, a mutant in all five PM-PINs could not form WiR, suggesting that these are the key factors involved in channeling auxin to the site of root initiation.

Another possible model is that PM-PIN localization is controlled by rates of cytoplasmic streaming, which are disrupted in *ro/big* mutants. PM-PINs are cycled in vesicles between the PM and endosomal compartments (Geldner et al. 2001), and the movement of these vesicles relies on cytoplasmic streaming promoted by the activity of myosins XI (Peremyslov et al. 2015, Kurth et al. 2017). The function of cytoplasmic streaming is still enigmatic, but it was shown that altering streaming rates can alter the plant developmental plan, including altering the final size of plant cells and organs (Tominaga et al. 2013). The rates of streaming are regulated by cytoplasmic Ca^{2+} concentrations, and increased Ca^{2+} causes inhibition of intracellular movement due to disruption of myosin activity (Tominaga and Ito 2015). Mutants in *big* have low rates of cytoplasmic streaming and can even exhibit temporary arrest of the movement, at least as measured in epidermal cells. Furthermore, it was shown that *big* mutants have high cytoplasmic Ca^{2+} concentrations (Hearn et al. 2018).

The link between cytoplasmic streaming, calcium and auxin is complex. In plants, both auxin and injury or touch were shown to increase cytoplasmic Ca^{2+} concentration (Ayling and Clarkson 1996, Vanneste and Friml 2013, Kiep et al. 2015, Marhavý et al. 2019), and in the shoot meristem, these Ca^{2+}-induced signals were important for reorientation of PM-PIN proteins (Li et al. 2019). Auxin treatment was shown to increase rates of cytoplasmic streaming at low concentrations but inhibit it at higher concentrations (Ayling et al. 1994, Friml et al. 2022). Recently, it was shown that mutants that do not alter the rate of cytoplasmic streaming in response to auxin have lower rates of vasculature reconnection following injury, supporting the link between auxin response, cytoplasmic streaming and downstream developmental responses (Friml et al. 2022). Furthermore, mutants in *Arabidopsis* myosins XIs, which are defective in cytoplasmic streaming, also exhibit defects in PIN1 polarization. Consistently, auxin distribution in their roots resembled that of WT roots treated with NPA. Curiously, these mutants had increased, rather than decreased number of hypocotyl-derived roots. Exogenous auxin abolished the difference in root initiation between WT and myosin mutants, suggesting that altered auxin distribution is the cause of the phenotype (Abu-Abied et al. 2018).

Taken together, we hypothesize a possible model where the role of RO/BIG is to buffer increased cytoplasmic Ca^{2+} concentration triggered by auxin or other signals. This allows rapid streaming, the deployment of PIN proteins to the membrane and, thus, altered auxin transport rates (**Fig. 7L**). This proposed role for RO/BIG is consistent with the suggested role for UBR4 in neurons, where it is important for buffering the deleterious effects caused by increased concentration of cytoplasmic Ca^{2+} during neuronal activation (Belzil et al. 2013). However, further studies will be required to fully test this hypothesis.

Materials and Methods

Plant materials and growth conditions

Tomato (*S. lycopersicum*) WTs are from M82 or Earliana cultivars. Seeds were obtained from the Tomato Genetics Resource Center (Davis, CA, USA). Tomato seeds were sown in soil and grown in long-day light conditions (16 h:8 h, 22°C) for 4 weeks and then transferred to a greenhouse and grown under natural light conditions. All *A. thaliana* plants used in this study are in the Columbia (Col-0) background. *tir3-1* (Ruegger et al. 1997) plants were backcrossed to Col to segregate out the *gl1* mutation. Resequencing of the *tir3-1* allele indicated that the mutation is a C>T transition at position 9,286 that causes a stop codon in the eighth exon and not as previously reported (**Supplementary Fig. S1E**; Gil et al. 2001). PIN mutants such as *pin1-1 eir1-1 (pin2), eir1-1 pin3-3 pin4-2 pin7En* (Verna et al. 2019), *pin1-1 eir1-1 (pin2) pin3-3 pin4-2 pin7En* (Verna et al. 2019), *pin6 pin8-1* (Sawchuk et al. 2013), *pin5-5* (Mravec et al. 2009) and *pin5-5 pin6-2 pin8-1* (Le et al. 2014) and *DR5rev:3xVENUS-N7* (Heisler et al. 2005) were previously described.

WiR assay

Roots from 4-week-old tomato plants were completely removed by cutting 1–2 cm above the root–hypocotyl junction, and resulting explants were incubated on rooting media: double distilled water (ddW), 10 μM IAA (Sigma I2886), 2 mM $CaCl_2$, 2 mM $CaCl_2$ + 2 mM EGTA (Sigma MFCD00004291) and 500 μM $MgCl_2$ in transparent flasks. The rooting solution was refreshed every 2 d. Experiments were performed in three or four replicates. For the rooting experiments, *Arabidopsis* seeds were sown on half-strength Murashige and Skoog medium, 2% agar plates, stratified for 3 d at 4°C in the dark and then transferred to long-day light conditions (16 h:8 h, 22°C). Five-day-old

Arabidopsis seedlings were cut above the root–hypocotyl junction to remove the root, and the resulting explants were incubated on Petri dishes with Whatman paper and rooting solution [ddW, IAA, $CaCl_2$, $MgCl_2$, NPA (Chem Service N-12507) and 2,4-D (Sigma D7299)]. Between three and four independent replicates were done for each experiment, each one with at least 20 plants per genotype and condition.

AR induction in cotyledon explants

Seeds were surface sterilized by immersion in 30% commercial bleach for 25 min followed by three rinses with sterile distilled water and aseptically sown in TK4 medium supplemented with 2% sucrose and 0.8% agar in 90-mm Petri dishes. Cotyledons were excised from 7- to 8-day-old seedlings and placed with their abaxial surface in a TK4 medium containing 1.5 mM Ca^{2+} supplemented with 50 nM NAA in 90-mm Petri dishes. NAA was dissolved in dimethyl sulfoxide (DMSO) and added to the medium after autoclaving to obtain a final DMSO concentration of <0.05%. Cotyledon explants were incubated in a growth chamber at 23°C ± 1°C with a photoperiod of 16-h light/8-h darkness and a photon fluence rate of 100 μmol m^{-2} s^{-1}.

Cloning and transgenic plants

Binary plasmids were built through the Golden Gate cloning system as described in Werner et al. (2012). *BIG gene* fragments I, II, IV and V were synthesized by Syntezza Bioscience Ltd. (Jerusalem, Israel) in the pUC57-Kan backbone, and fragments III and VI were cloned in the pAGM1287 backbone (primer for III: GTCAATCTCGGGAAAGACAAAG and CCCAGGCTTATTTCTTCGGGCTTTG and Primer for VI: CGAGGTGGAGGAAGAGATAGC). All BIG fragments were assembled as follows: 2x35s:*BIGfragment*-mScarlet-i:HSPterm in pICH47761. *Solyc02g089260* CRISPR binary plasmid was assembled as described in Brooks et al. (2014) carrying two guides targeting the sequences GATACAAGATGCATGCTTCA and GTGGCTGTATCCACATTGTC in the N-terminal region of the gene, the kanamycin resistance cassette from pICSL70004 and the CRISPR/cas9 cassette from pICH47742::2x35S-5′UTR-hCas9(STOP)-NOST. Tomato M82 transformation was performed according to McCormick (1991).

IAA transport assay

Three hypocotyl sections (5 mm) from 7-week-old M82 and *ro* mutant plants were used for basipetal IAA transport assays as described earlier (Nicolás et al. 2007, Cano et al. 2018). Briefly, these explants were placed in an upright position on a 1% agar block, and a 5 μl drop of a 200-μM labeled IAA ($[^{13}C]_6C_4H_9NO_2$; OlChemIm, Olomuc, Czech Republic) solution was added to the upper cut end. Every 30 min and up to 240 min, the receiver agar block was collected and replaced by a new one. During the assay, explants were kept in darkness at 25°C. Ten microliters of filtered extract was injected in a Ultra-Performace Liquid Chromatography-High-Resolution Mass Spectrometry (UPLC-HRMS) system consisting of an Acquity UPLC (Waters Corporation, Mildford, MA, USA) coupled to a Xevo G2-XS QToF mass spectrometer (Waters Corporation, Mildford, MA, USA) using an electrospray ionization interface. Mass spectra were obtained using the MassLynx software version 4.2 (Waters Corporation, Mildford, MA, USA). For IAA quantification, a calibration curve was constructed (1, 10, 50 and 100 μg l^{-1}). $[^{13}C_6]$-IAA was identified by extracting the exact mass from the full scan chromatogram obtained in the negative mode, adjusting a mass tolerance of ≤1 ppm. The concentrations of $[^{13}C_6]$-IAA were semi-quantitatively determined from the extracted area of the peak with the TargetLynx application manager (Waters Corporation, Mildford, MA, USA) by using the calibration curve of IAA. Each point on the curves corresponds to the mean ± SE. Linear traces of cumulative transported IAA were used to estimate transport intensity and velocity (Cano et al. 2018).

Transient expression on *Arabidopsis*

Three/four-day-old *Arabidopsis* seedlings were transformed with *Agrobacterium* using the Fast Agro-mediated Seedling Transformation technique (Li and Nebenführ 2010) with the Golgi marker (Man49-YFP; Nelson et al. 2007), the ER marker [green fluorescent protein (GFP)/YFP–HDEL; Nelson et al. 2007], vesicle marker (ARA6–GFP; Ueda et al. 2001) and/or *BIGfragment*-mScarlet-i.

Imaging

Tomato hypocotyls were hand-sections using a razor, stained with SR2200 [0.1% (v/v)] and mounted in water. *Arabidopsis* epidermal cotyledon cells were mounted in water. Tissue was observed using a Leica SP8 confocal microscope with 20× dry or 63× water objectives. Lasers of 405, 488 and 552 nm were used for excitation of SR2200, GFP/YFP and mScarlet-i, respectively. To visualize DR5 in *Arabidopsis* hypocotyls, tissue was cleared with ClearSee (Kurihara et al. 2015) and photographed using a Nikon SMZ18 fluorescence stereoscope with a 480-nm excitation/525/36-nm emission filters.

Immunohistochemistry

Roots from 6–9-day-old seedlings were cut and incubated for 16 h (overnight) in a TK4 liquid medium (control one with 1.5 mM $CaCl_2$ and without Ca^{2+}). Roots were fixed and subjected to a standard immunolocalization procedure using PIN1 (7E7F) antibody (1:40 dilution) (incubation overnight with primary antibody at 4°C and 1 h at 32°C). Roots were mounted on slides with a double spacer (300 μm total thickness) and scanned with a Leica Stellaris microscope (e.g. 488, 515–550 emission) with a constant setting for all samples. The images were exported to TIFF, and the fluorescence was measured with the Fiji program.

Measurement of vesicles and Golgi bodies movement

For analysis of cytoplasmic streaming, 20–60-s movies (≈1 frame/s) of *Arabidopsis* cotyledons expressing the Man49-YFP Golgi marker or ARA6-GFP vesicle marker were recorded using an SP8 confocal microscope with 63× water lens. Time-lapse images were examined to verify that tracked organelles are not moving out of plane. Only movies with at least 10 informative frames were used. For automatic extraction movement rates, movies were processed using TrackMate (Tinevez et al. 2017) in ImageJ software Fiji (Schindelin et al. 2012) using default parameters. Each movie resulted in 100–150 individual movement tracks. Density plots for movement rate distribution were generated using R 3.5.2.

Supplementary Data

Supplementary data are available at *PCP* online.

Data Availability

The data underlying this article are available in the article and in its online supplementary materials.

Funding

HHMI International Research Scholar grant (55008730) to I.E.; Israeli Science Foundation (ISF966/17) to I.E; Ministerio de Ciencia e Innovación of Spain (RTI2018-096505-B-I00) to J.M.P.-P; Conselleria d'Educació, Cultura i Sport of the Generalitat Valenciana (PROMETEO/2019/117) to J.M.P.-P; European Regional Development Fund of the European Commission to J.M.P.-P.

Acknowledgements

We would like to thank Einat Sadot for critical reading of this manuscript, Ziva Amsellem for assistance with tissue culture, Jiří Friml for providing materials and José Luis Micol for equipment.

Disclosures

The authors have no conflicts of interest to declare.

References

Abas, L., Kolb, M., Stadlmann, J., Janacek, D.P., Lukic, K., Schwechheimer, C., et al. (2021) Naphthylphthalamic acid associates with and inhibits PIN auxin transporters. *Proc. Natl. Acad. Sci. U.S.A.* 118: e2020857118.

Abu-Abied, M., Belausov, E., Hagay, S., Peremyslov, V., Dolja, V. and Sadot, E. (2018) Myosin XI-K is involved in root organogenesis, polar auxin transport, and cell division. *J. Exp. Bot.* 69: 2869–2881.

Adamowski, M. and Friml, J. (2015) PIN-dependent auxin transport: action, regulation, and evolution. *Plant Cell* 27: 20–32.

Ahkami, A.H., Melzer, M., Ghaffari, M.R., Pollmann, S., Ghorbani Javid, M., Shahinnia, F., et al. (2013) Distribution of indole-3-acetic acid in Petunia hybrida shoot tip cuttings and relationship between auxin transport, carbohydrate metabolism and adventitious root formation. *Planta* 238: 499–517.

Alaguero-Cordovilla, A., Sánchez-García, A.B., Ibáñez, S., Albacete, A., Cano, A., Acosta, M., et al. (2021) An auxin-mediated regulatory framework for wound-induced adventitious root formation in tomato shoot explants. *Plant Cell Environ.* 44: 1642–1662.

Ansari, S.A. and Kumar, P. (1994) IAA synergism and vitamin B1 antagonism with calcium for induction and growth of adventitious roots in branch cuttings of *Dalbergia sissoo* Roxb. *Indian J. Exp. Biol.* 32: 441–2.

Ayling, S.M., Brownlee, C. and Clarkson, D.T. (1994) The cytoplasmic streaming response of tomato root hairs to auxin; observations of cytosolic calcium levels. *J. Plant Physiol.* 143: 184–188.

Ayling, S.M. and Clarkson, D.T. (1996) The cytoplasmic streaming response of tomato root hairs to auxin; the role of calcium. *Funct. Plant Biol.* 23: 699–708.

Bellamine, J., Penel, C., Greppin, H. and Gaspar, T. (1998) Confirmation of the role of auxin and calcium in the late phases of adventitious root formation. *Plant Growth Regul.* 26: 191–194.

Bellini, C., Pacurar, D.I.I. and Perrone, I. (2014) Adventitious roots and lateral roots: similarities and differences. *Annu. Rev. Plant Biol.* 65: 639–666.

Belzil, C., Neumayer, G., Vassilev, A.P., Yap, K.L., Konishi, H., Rivest, S., et al. (2013) A Ca^{2+}-dependent mechanism of neuronal survival mediated by the microtubule-associated protein p600. *J. Biol. Chem.* 288: 24452–24464.

Boerjan, W., Cervera, M.T., Delarue, M., Beeckman, T., Dewitte, W., Bellini, C., et al. (1995) Superroot, a recessive mutation in *Arabidopsis*, confers auxin overproduction. *Plant Cell* 7: 1405–1419.

Brooks, C., Nekrasov, V., Lippman, Z.B. and Van Eck, J. (2014) Efficient gene editing in tomato in the first generation using the clustered regularly interspaced short palindromic repeats/CRISPR-associated9 system. *Plant Physiol.* 166: 1292–1297.

Butler, L. (1954) Two new mutants in the tomato propeller and rosette. *J. Heredity* 45: 25–27.

Cano, A., Sánchez-García, A.B., Albacete, A., González-Bayón, R., Justamante, M.S., Ibáñez, S., et al. (2018) Enhanced conjugation of auxin by GH3 enzymes leads to poor adventitious rooting in carnation stem cuttings. *Front. Plant Sci.* 9: 1–17.

da Costa, C.T., Offringa, R. and Fett-Neto, A.G. (2020) The role of auxin transporters and receptors in adventitious rooting of *Arabidopsis thaliana* pre-etiolated flooded seedlings. *Plant Sci.* 290: 110294.

de Klerk, G.-J., van der Krieken, W. and de Jong, J.C. (1999) The formation of adventitious roots: new concepts, new possibilities. *Vitro Cellular Dev. Biol. Plant* 35: 189–199.

Delarue, M., Prinsen, E., Van Onckelen, H., Caboche, M. and Bellini, C. (1998) Sur2 mutations of *Arabidopsis thaliana* define a new locus involved in the control of auxin homeostasis. *Plant J.* 14: 603–611.

Della Rovere, F., Fattorini, L., Ronzan, M., Falasca, G. and Altamura, M.M. (2016) The quiescent center and the stem cell niche in the adventitious roots of *Arabidopsis thaliana*. *Plant Signal. Behav.* 11: e1176660.

Desgagné-Penix, I., Eakanunkul, S., Coles, J.P., Phillips, A.L., Hedden, P. and Sponsel, V.M. (2005) The auxin transport inhibitor response 3 (tir3) allele of BIG and auxin transport inhibitors affect the gibberellin status of *Arabidopsis*. *Plant J.* 41: 231–242.

Dodd, A.N., Kudla, J. and Sanders, D. (2010) The language of calcium signaling. *Annu. Rev. Plant Biol.* 61: 593–620.

Druege, U., Franken, P. and Hajirezaei, M.R. (2016) Plant hormone homeostasis, signaling, and function during adventitious root formation in cuttings. *Front. Plant Sci.* 7: 1–14.

Friml, J., Gallei, M., Gelová, Z., Johnson, A., Mazur, E., Monzer, A., et al. (2022) ABP1–TMK auxin perception for global phosphorylation and auxin canalization. *Nature* 609: 575–581.

Geldner, N., Friml, J., Stierhof, Y.-D., Jürgens, G. and Palme, K. (2001) Auxin transport inhibitors block PIN1 cycling and vesicle trafficking. *Nature* 413: 425–428.

Gil, P., Dewey, E., Friml, J., Zhao, Y., Snowden, K.C., Putterill, J., et al. (2001) BIG: A calossin-like protein required for polar auxin transport in *Arabidopsis*. *Genes Dev.* 15: 1985–1997.

Guan, L., Tayengwa, R., Cheng, Z.M., Peer, W.A., Murphy, A.S. and Zhao, M. (2019) Auxin regulates adventitious root formation in tomato cuttings. *BMC Plant Biol.* 19: 1–16.

Gutierrez, L., Bussell, J.D., Pacurar, D.I., Schwambach, J., Pacurar, M. and Bellini, C. (2009) Phenotypic plasticity of adventitious rooting in *Arabidopsis* is controlled by complex regulation of AUXIN RESPONSE FACTOR transcripts and microRNA abundance. *Plant Cell* 21: 3119–3132.

Hearn, T.J., Ruiz, M.C.M., Abdul-Awal, S.M., Wimalasekera, R., Stanton, C.R., Haydon, M.J., et al. (2018) BIG regulates dynamic adjustment of circadian period in *Arabidopsis thaliana*. *Plant Physiol.* 178: 358–371.

Heisler, M.G., Ohno, C., Das, P., Sieber, P., Reddy, G.V., Long, J.A., et al. (2005) Patterns of auxin transport and gene expression during primordium development revealed by live imaging of the *Arabidopsis* inflorescence meristem. *Curr. Biol.* 15: 1899–1911.

Jarvis, B.C. and Yasmin, S. (1985) The influence of calcium on adventitious root development in mung bean cuttings. *Biochem. Physiol. Pflanz.* 180: 697–701.

Kalra, G. and Bhatia, S.C. (1998) Auxin-calcium interaction in adventitious root formation in the hypocotyl explants of sunflower (*Helianthus annuus* L.). *J. Plant Biochem. Biotechnol.* 7: 107–110.

Kanyuka, K., Praekelt, U., Franklin, K.A., Billingham, O.E., Hooley, R., Whitelam, G.C., et al. (2003) Mutations in the huge *Arabidopsis* gene BIG affect a range of hormone and light responses. *Plant J.* 35: 57–70.

Kiep, V., Vadassery, J., Lattke, J., Maaß, J.P., Boland, W., Peiter, E., et al. (2015) Systemic cytosolic Ca^{2+} elevation is activated upon wounding and herbivory in *Arabidopsis*. *New Phytol.* 207: 996–1004.

Kurihara, D., Mizuta, Y., Sato, Y. and Higashiyama, T. (2015) ClearSee: a rapid optical clearing reagent for whole-plant fluorescence imaging. *Development* 142: 4168–4179.

Kurth, E.G. Peremyslov, V.V., Turner, H.L., Makarova, K.S., Iranzo, J., Mekhedov, S.L., et al. (2017) Myosin-driven transport network in plants. *Proc. Natl. Acad. Sci.* 114: E1385–E1394.

Lakehal, A. and Bellini, C. (2019) Control of adventitious root formation: insights into synergistic and antagonistic hormonal interactions. *Physiol. Plant.* 165: 90–100.

Lanteri, M.L., Pagnussat, G.C. and Lamattina, L. (2006) Calcium and calcium-dependent protein kinases are involved in nitric oxide- and auxin-induced adventitious root formation in cucumber. *J. Exp. Bot.* 57: 1341–1351.

Le, J., Liu, X.G., Yang, K.Z., Chen, X.L., Zou, J.J., Wang, H.Z., et al. (2014) Auxin transport and activity regulate stomatal patterning and development. *Nat. Commun.* 5: 1–8.

Lee, H.W., Cho, C., Pandey, S.K., Park, Y., Kim, M.J. and Kim, J. (2019) LBD16 and LBD18 acting downstream of ARF7 and ARF19 are involved in adventitious root formation in *Arabidopsis*. *BMC Plant Biol.* 19: 1–11.

Li, J.F. and Nebenführ, A. (2010) FAST technique for *Agrobacterium*-mediated transient gene expression in seedlings of *Arabidopsis* and other plant species. *Cold Spring Harb. Protoc.*, pdb–prot5428.

Li, S.-W. and Xue, L. (2010) The interaction between H_2O_2 and NO, Ca^{2+}, cGMP, and MAPKs during adventitious rooting in mung bean seedlings. *Vitro Cellular Dev. Biol. Plant* 46: 142–148.

Li, T., Yan, A., Bhatia, N., Altinok, A., Afik, E., Durand-Smet, P., et al. (2019) Calcium signals are necessary to establish auxin transporter polarity in a plant stem cell niche. *Nat. Commun.* 10: 1–9.

Liu, Z., Zhang, R.-X., Duan, W., Xue, B., Pan, X., Li, S., et al. (2022) BIG modulates stem cell niche and meristem development via SCR/SHR pathway in *Arabidopsis* roots. *Int. J. Mol. Sci.* 23: 6784.

Marhavý, P., Kurenda, A., Siddique, S., Dénervaud Tendon, V., Zhou, F., Holbein, J., et al. (2019) Single-cell damage elicits regional, nematode-restricting ethylene responses in roots. *EMBO J.* 38: e100972.

McCormick, S. (1991) Transformation of tomato with *Agrobacterium tumefaciens*. *In* Plant Tissue Culture Manual. pp. 311–319. Springer, Dordrecht.

Mravec, J., Skůpa, P., Bailly, A., Hoyerová, K., Křeček, P., Bielach, A., et al. (2009) Subcellular homeostasis of phytohormone auxin is mediated by the ER-localized PIN5 transporter. *Nature* 459: 1136–1140.

Nakatani, Y., Konishi, H., Vassilev, A., Kurooka, H., Ishiguro, K., Sawada, J., et al. (2005) P600, a unique protein required for membrane morphogenesis and cell survival. *Proc. Natl. Acad. Sci. U.S.A.* 102: 15093–15098.

Nelson, B.K., Cai, X. and Nebenführ, A. (2007) A multicolored set of in vivo organelle markers for co-localization studies in *Arabidopsis* and other plants. *Plant J.* 51: 1126–1136.

Nicolás, J.I.L., Acosta, M. and Sánchez-Bravo, J. (2007) Variation in indole-3-acetic acid transport and its relationship with growth in etiolated lupin hypocotyls. *J. Plant Physiol.* 164: 851–860.

Niu, L., Yu, J., Liao, W., Yu, J., Zhang, M. and Dawuda, M.M. (2017) Calcium and calmodulin are involved in nitric oxide-induced adventitious rooting of cucumber under simulated osmotic stress. *Front. Plant Sci.* 8: 1684.

Omary, M., Gil-Yarom, N., Yahav, C., Steiner, E. and Efroni, I. (2022) A conserved superlocus regulates above- and belowground root initiation. *Science* 375: eabf4368.

Pacurar, D.I., Perrone, I. and Bellini, C. (2014) Auxin is a central player in the hormone cross-talks that control adventitious rooting. *Physiol. Plant.* 151: 83–96.

Peremyslov, V.V., Cole, R.A., Fowler, J.E. and Dolja, V.V. (2015) Myosin-powered membrane compartment drives cytoplasmic streaming, cell expansion and plant development. *PLoS One* 10: e0139331.

Ruegger, M., Dewey, E., Hobbie, L., Brown, D., Bernasconi, P., Turner, J., et al. (1997) Reduced naphthylphthalamic acid binding in the tir3 mutant of *Arabidopsis* is associated with a reduction in polar auxin transport and diverse morphological defects. *Plant Cell* 9: 745–757.

Sabatini, S., Beis, D., Wolkenfelt, H., Murfett, J., Guilfoyle, T., Malamy, J., et al. (1999) An auxin-dependent distal organizer of pattern and polarity in the *Arabidopsis* root. *Cell* 99: 463–472.

Saint-Jore-Dupas, C., Nebenführ, A., Boulaflous, A., Follet-Gueye, M.-L., Plasson, C., Hawes, C., et al. (2006) Plant N-glycan processing enzymes employ different targeting mechanisms for their spatial arrangement along the secretory pathway. *Plant Cell* 18: 3182–3200.

Sauer, M. and Kleine-Vehn, J. (2019) PIN-FORMED and PIN-LIKES auxin transport facilitators. *Development* 146: dev168088.

Sawchuk, M.G., Edgar, A. and Scarpella, E. (2013) Patterning of leaf vein networks by convergent auxin transport pathways. *PLoS Genet.* 9: 1003294.

Schiefeibein, J.W., Benfeyb, P.N., Schiefelbein, J.W. and Benfey, P.N. (1991) The development of plant roots: new approaches to underground problems. *Plant Cell* 3: 1147–1154.

Schindelin, J., Arganda-Carreras, I., Frise, E., Kaynig, V., Longair, M., Pietzsch, T., et al. (2012) Fiji: an open-source platform for biological-image analysis. *Nat. Methods* 9: 676–682.

Shim, S.Y., Wang, J., Asada, N., Neumayer, G., Tran, H.C., Ishiguro, K.I., et al. (2008) Protein 600 is a microtubule/endoplasmic reticulum-associated protein in CNS neurons. *J. Neurosci.* 28: 3604–3614.

Simon, S., Skůpa, P., Viaene, T., Zwiewka, M., Tejos, R., Klíma, P., et al. (2016) PIN6 auxin transporter at endoplasmic reticulum and plasma membrane mediates auxin homeostasis and organogenesis in *Arabidopsis*. *New Phytol.* 211: 65–74.

Sparkes, I.A., Ketelaar, T., De Ruijter, N.C.A. and Hawes, C. (2009) Grab a golgi: laser trapping of golgi bodies reveals in vivo interactions with the endoplasmic reticulum. *Traffic* 10: 567–571.

Steffens, B. and Rasmussen, A. (2016) The physiology of adventitious roots. *Plant Physiol.* 170: 603–617.

Sukumar, P., Maloney, G.S. and Muday, G.K. (2013) Localized induction of the ATP-binding cassette B19 auxin transporter enhances adventitious root formation in *Arabidopsis*. *Plant Physiol.* 162: 1392–1405.

Swarup, R. and Péret, B. (2012) AUX/LAX family of auxin influx carriers—an overview. *Front. Plant Sci.* 3: 1–11.

Teale, W. and Palme, K. (2018) Naphthylphthalamic acid and the mechanism of polar auxin transport. *J. Exp. Bot.* 69: 303–312.

Teale, W.D., Pasternak, T., Dal Bosco, C., Dovzhenko, A., Kratzat, K., Bildl, W., et al. (2021) Flavonol-mediated stabilization of PIN efflux complexes regulates polar auxin transport. *EMBO J.* 40: 1–14.

Tinevez, J.Y., Perry, N., Schindelin, J., Hoopes, G.M., Reynolds, G.D., Laplantine, E., et al. (2017) TrackMate: An open and extensible platform for single-particle tracking. *Methods* 115: 80–90.

Tominaga, M. and Ito, K. (2015) The molecular mechanism and physiological role of cytoplasmic streaming. *Curr. Opin. Plant Biol.* 27: 104–110.

Tominaga, M., Kimura, A., Yokota, E., Haraguchi, T., Shimmen, T., Yamamoto, K., et al. (2013) Cytoplasmic streaming velocity as a plant size determinant. *Dev. Cell* 27: 345–352.

Ueda, T., Yamaguchi, M., Uchimiya, H. and Nakano, A. (2001) Ara6, a plant-unique novel type Rab GTPase, functions in the endocytic pathway of *Arabidopsis thaliana*. *EMBO J.* 20: 4730–41.

Ulmasov, T., Murfett, J., Hagen, G. and Guilfoyle, T.J. (1997) Aux/IAA proteins repress expression of reporter genes containing natural and highly active synthetic auxin response elements. *Plant Cell* 9: 1963–1971.

Ung, K.L., Winkler, M., Schulz, L., Kolb, M., Janacek, D.P., Dedic, E., et al. (2022) Structures and mechanism of the plant PIN-FORMED auxin transporter. *Nature* 609: 605–610.

Vanneste, S. and Friml, J. (2013) Calcium: the missing link in auxin action. *Plants* 2: 650–675.

Verna, C., Ravichandran, S.J., Sawchuk, M.G., Linh, N.M., Scarpella, E., Linh, M., et al. (2019) Coordination of tissue cell polarity by auxin transport and signaling. *eLife* 8: e51061.

Weijers, D. and Wagner, D. (2016) Transcriptional responses to the auxin hormone. *Annu. Rev. Plant Biol.* 67: 539–574.

Welander, M., Geier, T., Smolka, A., Ahlman, A., Fan, J. and Zhu, L.H. (2014) Origin, timing, and gene expression profile of adventitious rooting in *Arabidopsis* hypocotyls and stems. *Am. J. Bot.* 101: 255–266.

Werner, S., Engler, C., Weber, E., Gruetzner, R. and Marillonnet, S. (2012) Fast track assembly of multigene constructs using Golden Gate cloning and the MoClo system. *Bioeng. Bugs.* 3: 38–43.

Xu, M., Zhu, L., Shou, H. and Wu, P. (2005) A PIN1 family gene, OsPIN1, involved in auxin-dependent adventitious root emergence and tillering in rice. *Plant Cell Physiol.* 46: 1674–1681.

Yang, H. and Murphy, A.S. (2009) Functional expression and characterization of *Arabidopsis* ABCB, AUX 1 and PIN auxin transporters in *Schizosaccharomyces pombe*. *Plant J.* 59: 179–191.

Yu, J.J., Niu, L., Yu, J.J., Liao, W., Xie, J., Lv, J., et al. (2019) The involvement of ethylene in calcium-induced adventitious root formation in cucumber under salt stress. *Int. J. Mol. Sci.* 20: 1047.

Zhao, Y. (2014) Auxin biosynthesis. *Arabidopsis Book* 12: e0173.

Zobel, R.W. (1975) The genetics of root development. *In* The Development and Function of Roots. Edited by Torrey, J. and Clarkson, D. pp. 261–275. Academic Press, London.